Qualitative *ab initio* theory of magnetic and atomic ordering in FeNi

A. V. Ruban

Department of Materials Science and Engineering, KTH Royal Institute of Technology, SE-100 44 Stockholm, Sweden and Materials Center Leoben Forschung GmbH, A-8700 Leoben, Austria

(Received 4 December 2023; revised 25 January 2024; accepted 4 March 2024; published 15 March 2024)

Magnetic and atomic ordering in equiatomic FeNi alloy is studied by different *ab initio* techniques and methods based on density functional theory in order to clarify the main driving forces and their interplay behind these transitions and possibility of their accurate description within standard density functional theory calculations. The Curie temperature is obtained in Monte Carlo simulations using magnetic exchange interactions obtained by applying the magnetic force theorem within multiple scattering theory for different magnetic and atomic configurational states, including account for the thermal atomic displacements and exchange-correlation potential. The calculations show a very strong sensitivity of the results upon exchange-correlation potential, atomic order, and thermal atomic displacements. The calculated Curie temperature of a completely random alloy with the account of thermal lattice displacement is at least about 200 K below the known experimental data (780–800 K) depending on the above mentioned factors. The atomic order-disorder transition temperature is determined from effective chemical interactions, which apart from the chemical contribution (on the ideal fcc lattice) include contributions from lattice thermal vibrations and local lattice relaxations. The effective chemical interactions are strongly affected by the magnetic state, so the order-disorder transition temperature changes between 1000 and 140 K in the fully ordered ferromagnetic and paramagnetic states, respectively. For the reduced magnetization 0.7 (close to the experimental order-disorder transition temperature at 600 K), the order-disorder transition temperature varies between 550 and 700 K depending mostly on the exchange-correlation potential. The latter effect is the uncertainty in the choice of the exchange-correlation approximation in density functional theory calculations.

DOI: 10.1103/PhysRevB.109.094108

I. INTRODUCTION

Fe-Ni alloys are known for their fascinating properties related to magnetism. Invar and Elinvar alloys containing approximately 35 at. % of Ni are probably the most well known among materials science community. On the other side of the alloy compositions, with approximately 20 at. % of Fe, there exists permalloy known for its very high magnetic permeability, very low magnetostriction, and large anisotropic magnetoresistance, which makes this alloy indispensable in diverse applications. Both these alloys were developed about 100 years ago.

Equiatomic random Fe-Ni alloys (sometimes called "taenite") are magnetically soft, and they have not been of much interest until recently, when it was discovered that the FeNi-$L1_0$ ordered phase ("tetrataenite") has large magnetic anisotropy, so it could be used in permanent magnets instead of expensive platinum-group or rare-earth metals (see, for instance, Ref. [1]). A fascinating story of the discovery of FeNi-$L1_0$ in meteorites and its experimental investigation can be found, for instance, in Ref. [2]. There is considerable interest in making the tetrataenite industrially available [3].

The FeNi-$L1_0$ ordered phase (tetrataenite) was first obtained in neutron irradiation experiments under magnetic fields [4]. The order-disorder transition temperature was determined to be 590 K, at which diffusion becomes very sluggish, making it extremely difficult to obtain the ordered phase without special treatments. The order-disorder transition happens in the ferromagnetic (FM) state with reduced magnetization of about 0.7 [5] (at 600 K). The Curie temperature of random FeNi alloys is close to 780 K (there is no certain value: it depends on the atomic configuration, 780 K [5] or 775 K [6]) in random alloys, while it ranges from 800 to 848 K for the $L1_0$-ordered FeNi alloys in meteoritic samples [2,7,8].

Magnetic and atomic ordering transitions in this alloy have been investigated in a number of first-principles studies [9–12]. In spite of the fact that the ordering temperatures obtained in some of them are spectacularly close to the experimental data [11,12], there remain some controversial issues related to the effect of magnetism and thermal lattice vibrations upon order-disorder phase transition in these theoretical investigations.

In particular, as has been found in first-principles based mean-field modeling in Ref. [11], the vibrational contribution obtained using the Debye-Grüneisen model lowers the transition temperature from about 1000 K to approximately

600 K. Similar results were obtained in Ref. [12], where the vibrational contribution obtained was in the *ab initio* phonon calculations, which then were included in the cluster expansion. At the same time, according to another first-principles investigation based on the Debye-Grüneisen model [9], the vibrational contribution lowers the order-disorder transition temperature only by 40 K: from 520 to 480 K. Of course, in all these investigations, the methods used were quite different and all of them are based on certain approximations. Nevertheless, such a large vibrational effect obtained in Refs. [11,12] is quite unusual.

Another controversial point concerns the "interplay" between magnetism and ordering. As has been determined in earlier *ab initio* investigations, ferromagnetism promotes ordering tendency in both Fe-rich [13] and Ni-rich [14] Fe-Ni alloys. In the latter case, the magnetic state effect is especially large: the order-disorder transition temperature in the paramagnetic (PM) state is about 400 K lower than in the FM state. This is not what is found in Ref. [12]: although the order-disorder transition temperature in Ni_3Fe is about 170 K higher in the FM state than in the PM one, the effect of the magnetic state is reversed in FeNi: according to Ref. [12], ferromagnetism lowers the order-disorder phase transition by about 50 K (compared to the PM state). This result is difficult to reconcile with the above mentioned experimental observations that the Curie temperature in the ordered FeNi alloys is greater than that in random alloys.

In this paper, a density-functional theory (DFT) based modeling of both magnetic and atomic ordering transitions is performed with the aim of getting a clearer picture of the main driving forces behind these transitions in FeNi. Such a modeling can be only qualitative, apart from the fact that phase transition (magnetic or atomic ordering) temperatures are generally very difficult to obtain accurately for any kind of systems, due to their sensitivity to many factors, which are still hard, if possible at all, to model with the required precision. Moreover, there are no DFT tools that can capture the energetics of FeNi in the whole range of relevant temperatures, properly taking into consideration the corresponding magnetic, chemical, and vibrational excitations. The range of uncertainties (error bars) in the DFT based calculations of phase transitions in FeNi is not known. This paper is an attempt to determine it as well as the source of errors whenever possible.

Although the finite-temperature magnetism and electronic structure can be more reliably and accurately obtained using, for instance, dynamical mean-field theory (DMFT) [15,16], such methods are impractical for total energy calculations of large supercells needed in the modeling of random alloys. Nevertheless, the level of accuracy of the present DFT modeling is good enough to establish a qualitative picture of the forces behind magnetic and atomic ordering transitions in this alloy.

II. METHODOLOGY

A. Alloy configurational Hamiltonian

The following configurational Hamiltonian has been used in statistical thermodynamics simulations of the order-disorder phase transition:

$$H^{\rm all} = \frac{1}{2}\sum_p V_p^{(2)} \sum_{ij\in p} \delta c_i \delta c_j + \frac{1}{3}\sum_t V_t^{(3)} \sum_{i,j,k} \delta c_i \delta c_j \delta c_k \times \frac{1}{4}\sum_q V_q^{(4)} \sum_{i,j,k,l} \delta c_i \delta c_j \delta c_k \delta c_l. \quad (1)$$

Here, the summation is performed over different types of clusters (p, t, and q), and lattice sites (i, j, k, and l); $V_p^{(2)}$, $V_t^{(3)}$, and $V_q^{(4)}$ are the pair, three-site, and four-site effective interactions for corresponding clusters (p, t, and q). In the case of equiatomic alloy composition, three-site interactions practically do not contribute to the alloy energetics and therefore they have not been considered in the statistical simulations, although they were obtained in *ab initio* calculations.

B. Magnetic Hamiltonian

The Heisenberg form of the magnetic Hamiltonian was used in this paper:

$$H^{\rm mag} = -\sum_p \sum_{\alpha,\beta={\rm Fe,Ni}} J_p^{\alpha,\beta} \sum_{ij\in p} \mathbf{e}_i \mathbf{e}_j c_i^\alpha c_j^\beta, \quad (2)$$

where magnetic exchange interactions $J_p^{\alpha,\beta}$ depend on the type of alloy components: α, β, and coordination shell p. $c_i^\alpha = 1$ if the α alloy component occupies site i, otherwise it is zero. In random alloy, $J_p^{\rm FeNi} = J_p^{\rm NiFe}$, however these are two different interactions in a partially ordered alloy. The details of obtaining the magnetic interactions are given below.

C. DFT electronic structure and total energy calculations

Two different techniques have been used in this investigation. The projector augmented wave (PAW) method [17] as implemented in the Vienna *Ab Initio* Simulation Package (VASP) [18–20] was used to get the DFT accurate total energies of a certain set of alloys as well as in the force constant calculations for vibrational properties of random and ordered alloys. All the PAW calculations were done using the generalized gradient approximation (GGA)–Perdew-Burke-Ernzerhof (PBE) exchange correlation potential and energy [21]. The kinetic energy cutoff was 350 eV except the force constant calculations, where it was 500 eV.

The Green's function multiple scattering technique (MST) was also used in the electronic structure, total energy, and magnetic and effective chemical interaction calculations of random and partially ordered alloys in different magnetic states. Such calculations have been done either using the coherent potential approximation (CPA) [22] or the locally self-consistent Green's function (LSGF) technique [23], which accurately accounts for the local environment effects in random alloys.

The MST techniques have been used within the exact muffin-tin orbital (EMTO) method [24,25] referenced here as EMTO-CPA [26] and ELSGF [27], respectively. The EMTO-CPA calculations have been done by the Lyngby version of the Green's function EMTO code [28], where the screened

Coulomb interactions in the single-site DFT-CPA approximation [29], the screened generalized perturbation method (SGPM) [30–32], and magnetic force theorem method [33,34] are implemented [35]. The MST self-consistent calculations were done using local spin-density approximation (LSDA) [36]. In some cases, the GGA-PBE self-consistent calculations were done for the magnetic exchange and effective chemical interactions.

The contributions of the screened Coulomb interactions to the one-electron potential of alloy components $V^i_{\rm scr}$ and total energy $E_{\rm scr}$ in the EMTO-CPA calculations were defined as [29]

$$v^i_{\rm scr} = -e^2\alpha^0\frac{\bar{q}_i}{S}, \quad E_{\rm scr} = \sum_i c_i E^i_{\rm scr},$$
$$E^i_{\rm scr} = -e^2\frac{1}{2}\alpha^0_i\beta_{\rm scr}\frac{q_i^2}{S}, \tag{3}$$

where q_i and α^0 are the net charge of the atomic sphere of the ith alloy component in the single-site CPA calculations and the on-site screening constant (one for a binary alloy), S is the Wigner-Seitz radius, and $\beta_{\rm scr}$ is the on-site screening constant, which accounts for the electrostatic multipole moment contribution to the electrostatic energy due to inhomogeneous local environment of different sites in a random alloy. Similarly, the contribution from the screened Coulomb interactions to the SGPM effective pair interactions at the pth coordination shell was calculated as

$$V^{\rm scr}_p = e^2\alpha_p\frac{\bar{q}^2}{S}, \tag{4}$$

where α_p is the intersite screening constant and $\bar{q}$ is the difference of the net charges of the atomic sphere of Fe and Ni.

The onsite and intersite screening constants, α^0 and α_p as well as the $\beta_{\rm scr}$ were determined in the ELSGF 1024-atom supercell calculations of random FeNi alloy in the FM and disordered local moment (DLM) states. The resulting screening constants turned out to be very little dependent on the magnetic state: $\alpha^0 = 0.79$ and 0.78 in the FM and PM states, respectively.

The MST-EMTO calculations of alloys in the finite-temperature PM state were done using DLM configuration treated within CPA [37,38]. Since DLM fails for Ni (local magnetic moments collapse), the longitudinal spin fluctuations (LSFs) at the given temperature were included, approximating the corresponding entropy t as [39]

$$S^{\rm LSF}_i = 3\ln m_i, \tag{5}$$

where m_i is the local magnetic moment of the ith site with Ni (or just the Ni component in the case of random alloy CPA calculations).

D. Corresponding state principle for the effective chemical and magnetic interactions for the phase transition calculations

The magnetic and atomic order-disorder transition temperatures were determined in Monte Carlo simulations with the magnetic and effective chemical interactions obtained at the conditions, which correspond to the experimental state of the alloy at the transition temperatures. In particular, the magnetic exchange interactions for the Curie temperature calculations (experimental value is close to 800 K) were obtained at the experimental 800 K lattice constant, 3.597 Å [40] in the PM state taking into consideration the corresponding electronic and magnetic (LSF) excitations at this temperature. The effective chemical interactions for the order-disorder phase transition (experimental value is about 600 K) were obtained at the experimental 600 K lattice constant (3.591 Å, from Ref. [40]) in the partially disordered magnetic state with a reduced magnetization of 0.7, which is close to experimental magnetization at 600 K [5].

As will be clear from the results presented below, this is a reasonable approach since magnetic and chemical interactions in this alloy are extremely sensitive to the magnetic state and the degree of atomic order. This makes an accurate and reliable fully self-consistent account of these degrees of freedom in statistical simulations of both transitions impossible. Although one could perform a "partial" consistency of the effective chemical interactions with the magnetization determined in magnetic simulations with a fixed set of magnetic interactions, like it was done in Ref. [14] in the modeling of the order-disorder phase transition in Ni_3Fe, it has not been done here since the reliable DFT calculations of the alloy magnetization below the Curie temperature (as well as the Curie temperature) are hardly possible.

E. DFT modeling of the finite-temperature magnetism in FeNi

Although it seems that DFT (or more strictly speaking the LSDA) yields very close results for the spin magnetic moments in both ordered and random FeNi [15], the account of electron correlations within the multiorbital Hubbard model in DMFT calculations leads to noticeable changes in the density of states, especially for Fe in the random alloy. To what extent this affects the energetics as well as magnetic and chemical interactions is not known. Can one still trust the DFT results for magnetic and chemical ordering temperatures within several degrees Kelvin under the condition that all the other effects are included properly in simulations? Definitely no. What is interesting, however, is what the error bar of DFT simulations is.

III. RESULTS

A. Magnetic exchange interactions and Curie temperature

FeNi alloys exhibit very complicated magnetism [41,42], which requires the use of a quite elaborate magnetic Hamiltonian in the whole range of temperatures. However, since the only purpose of the statistical simulations in this paper is to find the Curie temperature, a simple form of the Heisenberg magnetic Hamiltonian (2) can be used. The complex dependence of the magnetic interactions on the local and global magnetic state then can be reduced to just a single set of magnetic interactions in the PM state at the experimental Curie temperature and the corresponding lattice constant.

That is, it is tacitly assumed that the system can still be described by the usual Heisenberg Hamiltonian just close to the magnetic phase transition. At this point, the magnetic state can be considered as paramagnetic (with some magnetic short-range order (SRO), which is neglected in this paper in

TABLE I. Local magnetic moments (μ_B) of Fe and Ni in random and ordered FeNi alloy in the EMTO calculations obtained in the LSDA and GGA-PBE for the lattice constant of 3.597 Å. DLM-LSF calculations were done at 800 K.

	FM		DLM-LSF	
	LSDA	GGA	LSDA	GGA
	Random alloy			
Fe	2.49	2.56	2.12	2.30
Ni	0.71	0.71	0.64	0.66
	$L1_0$ ordered			
Fe	2.67	2.74	2.30	2.41
Ni	0.59	0.59	0.61	0.62

the calculations of the magnetic interactions). The magnetic exchange interactions were obtained using the magnetic force theorem [33–35]. In these calculations, Ni was described in the DLM-LSF model at $T = 800$ K.

To provide a better overview of all possible factors (on the DFT level) which can affect the results for the Curie temperature, the Monte Carlo simulations were also done with magnetic exchange interactions obtained in the FM state with different reduced magnetizations using two "popular" exchange-correlation potentials (LSDA and GGA-PBE) as well as varying the state of atomic order and using model supercells to account for the local environment effects (atomic short-range order).

1. Local environment effects in FeNi random alloy

As was noticed a long time ago [41], the Fe-Fe magnetic exchange interactions are extremely sensitive to the local environment of the atoms, which fluctuates from site to site in a random alloy. It is known (also observed in the present paper) that Fe atoms in Fe-Ni alloy totally surrounded by Fe atoms at the first coordination shell interact antiferromagnetically with their Fe nearest neighbors even in the FM state, and the direction of their magnetic moments is opposite to the global magnetization.

The magnetic moment of Fe (not so much of Ni) is also sensitive to the magnetic state, the atomic order, and the exchange-correlation potential used in the self-consistent calculations. These dependences are shown in Table I for the lattice constant of 3.597 Å. As one can see, the magnetic moment of Fe is indeed more sensitive to the variation of these parameters than that of Ni. The strongest effect is due to the magnetic state: The magnetic moment of Fe in the FM state is substantially larger than those in the PM DLM-LSF state. The state of the atomic order also affects the magnetic moment of Fe: It is larger in the $L1_0$ ordered alloy, where Fe atoms have fewer Fe nearest neighbors, than in the random one. Finally, the GGA-PBE magnetic moments are larger than the LSDA ones (as usual).

To study the effect of local chemical environment on the magnetic moments and magnetic exchange interactions, the EMTO LSDA self-consistent calculations were performed for a 64-atom supercell representing a random $Fe_{0.5}Ni_{0.5}$ alloy in the FM and DLM states. In the DLM calculations, all the sites were treated within the CPA as usual making random spin-up–spin-down configuration. In the case of Ni sites, additional LSF contribution at 800 K was added as described above. The effect of local chemical environment on the magnetic moment and magnetic exchange interactions of Ni atoms is rather weak. In contrast, it is very strong for Fe.

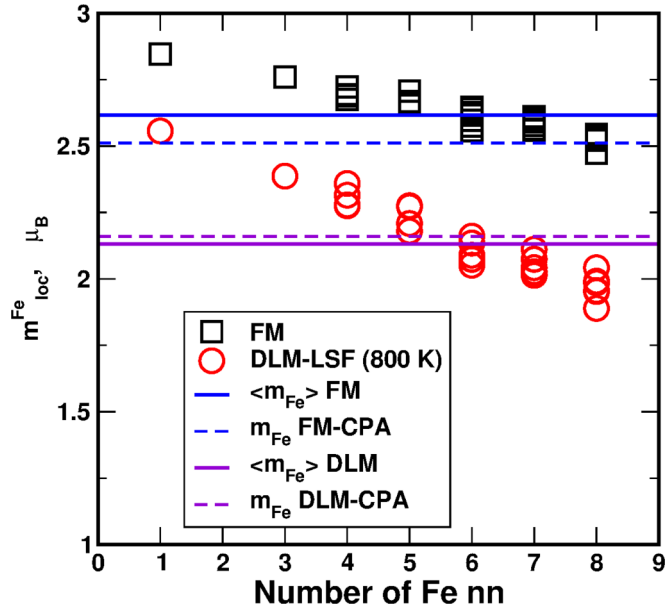

FIG. 1. Local magnetic Fe in random $Fe_{0.5}Ni_{0.5}$ alloy as a function of the number of Fe nearest neighbors.

In Fig. 1, the local magnetic moments of Fe atoms in the FM and DLM state are shown as a function of their Fe nearest neighbors. In both cases the local magnetic moment of Fe decreases almost linearly with the number of the Fe nearest neighbors, and such a decrease is more pronounced in the paramagnetic (DLM) state. The average results for magnetic moment (shown by bold lines) are close to those obtained in the CPA calculations representing an "isomorphous" model of a random alloy where all Fe and Ni atoms are the same.

Since the size of the supercell is relatively small (64 sites), there are no Fe atoms completely surrounded by Fe atoms. However, the calculations for larger supercells show that in such cases, the magnetic moment of Fe becomes antiferromagnetically aligned with the magnetic moments of the surrounding Fe atoms, as has been already mentioned above. It is also clear that in the DLM state the local magnetic moment of such Fe atoms should be quite small, exhibiting weak itinerant magnetism. This reveals an enormous complexity of the magnetism in this system: Fe atoms surrounded by Fe and Ni exhibit very different magnetic behaviors in the same alloy.

In contrast to the local magnetic moments, the local environment has a complex and unpredictable effect on the Fe-Fe magnetic exchange interactions, which vary widely in magnitude and sign. Figure 2 shows the Fe-Fe magnetic exchange interactions at the first coordination shell for the 64-atom $Fe_{0.5}Ni_{0.5}$ supercell in the FM (top) and paramagnetic DLM-LSF (bottom) states obtained using the formalism of the magnetic force theorem [33,34] within the EMTO-CPA method [35]. The results appear to be random. Interestingly,

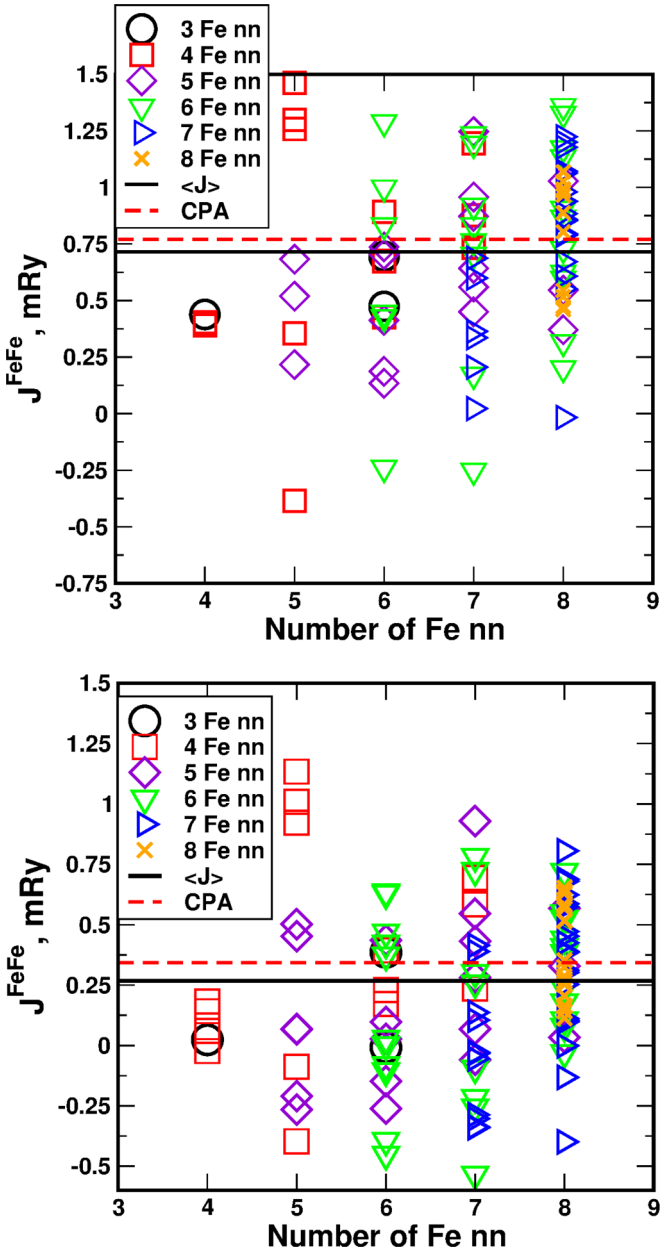

FIG. 2. The nearest neighbor Fe-Fe magnetic exchange interactions in $Fe_{0.5}Ni_{0.5}$ alloy in FM (top) and DLM (bottom) states.

the average interactions shown by solid lines are very similar to those obtained in the CPA calculations for $Fe_{0.5}Ni_{0.5}$ alloy. This suggests that the CPA can provide a reasonable mean-field approximation of the magnetism and interactions in the $Fe_{0.5}Ni_{0.5}$ random alloy.

One can also calculate "local and partial" J_0^i at site i either directly [34] as is done in this paper in the CPA calculations or using the equivalent definition:

$$J_0^i = \sum_j J_{ij}. \tag{6}$$

Here, the summation is done over all sites. In the case of elementary solids, it can be used for a mean-field estimate of the Curie temperature: $T_c = 2/3J_0$. In Fig. 3, such local J_0^i

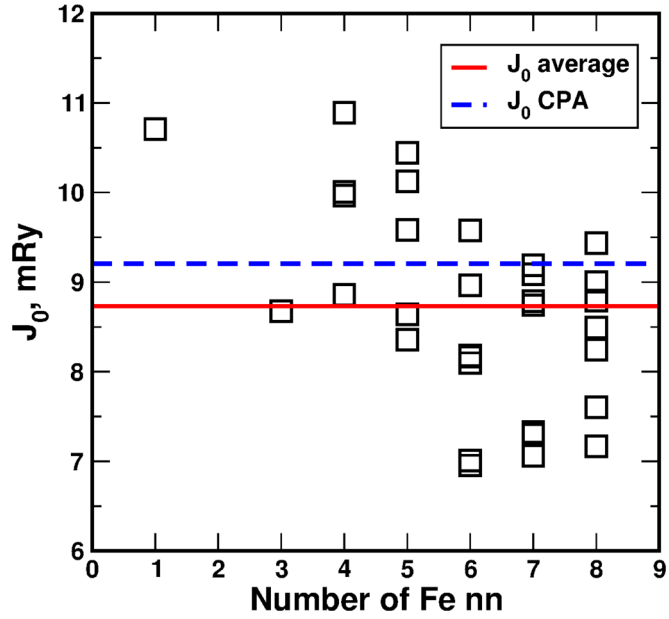

FIG. 3. Local J_0^i for Fe sites obtained for the 64-atom supercell as a function of the number of Fe nearest neighbors.

are shown for Fe atoms in the 64-atom supercell. Again, the results are quite scattered although it is clear that J_0^i is larger for Fe atoms mostly surrounded by Ni. The CPA J_0^{Fe} is also quite close to the average value of $\langle J_0^{i=Fe} \rangle$ in the supercell.

2. Curie temperature

Despite the strong local environment effect on the Fe-Fe magnetic exchange interactions, the Curie temperature is relatively insensitive to these fluctuations and can be reasonably estimated by the simplest CPA mean-field approach as shown below. This implies that the CPA magnetic exchange interactions capture the average behavior of such interactions in the alloy under the influence of various internal and external parameters.

Figure 4 shows the "CPA average" magnetic exchange interactions in random $Fe_{0.5}Ni_{0.5}$ alloy obtained in the LSDA EMTO-CPA calculations [35] in the FM and DLM-LSF states at the lattice constant of 3.597 Å. The interactions beyond the fourth coordination shell are relatively small in both cases. The magnetic state has a moderate effect on the Ni-Ni exchange interactions. However, the Fe-Fe and Fe-Ni exchange interactions differ significantly in the FM and DLM-LSF states: the Fe-Fe interactions dominate in the FM state, while the Fe-Ni interactions dominate in the DLM-LSF state.

The Curie temperature was determined in Heisenberg Monte Carlo simulations using these interactions. The simulation box had a size of $14\times14\times14(4)$—10 976 sites. Fe and Ni atoms were randomly distributed on the fcc underlying lattice, and the magnetic exchange interactions at the first ten coordination shells were used in the calculations. The heat capacity peak was used to identify the Curie temperature. The temperature step was 10 K, which is sufficient for the present semiqualitative analysis.

Table II shows the Curie temperatures calculated using different magnetic exchange interactions. The results indicate

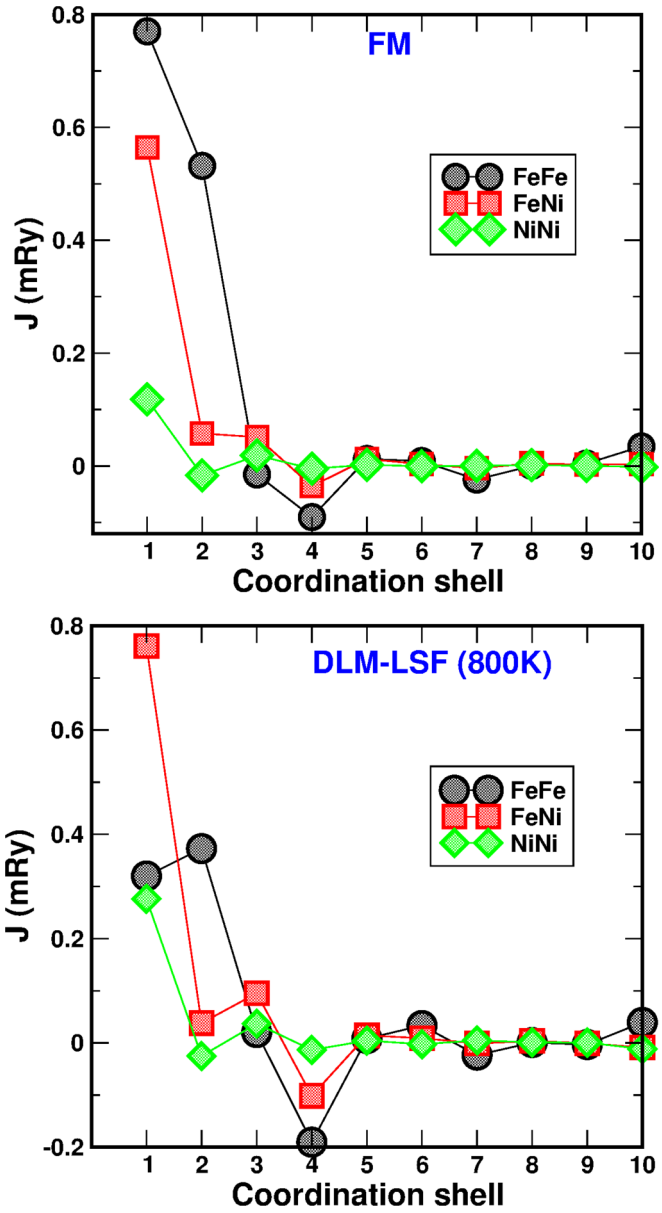

FIG. 4. J_{ij} in $Fe_{0.5}Ni_{0.5}$ random alloy obtained in the CPA calculations in the FM state (top) and in the paramagnetic DLM-LSF state at 800 K (bottom).

that the magnetic state (FM vs DLM-LSF) has a relatively small effect on the Curie temperature, while the choice of the exchange-correlation potential in the self-consistent calculations (the same lattice constant) has a stronger effect. It is known that GGA-PBE overestimates the magnetic moments of some 3*d* metals, especially of Fe. This is also true for FeNi as shown in Table I, where the magnetic moments of Fe and Ni are given for random and $L1_0$ ordered alloys obtained in the LSDA or GGA-PBE EMTO self-consistent calculations.

TABLE II. Curie temperature (in K) for different sets of magnetic interactions obtained in EMTO-CPA calculations for $Fe_{0.5}Ni_{0.5}$ alloy.

FM		DLM-LSF	
LSDA	GGA	LSDA	GGA
650	730	610	700

TABLE III. Curie temperature (in K) obtained in 32- and 64-atom supercell Monte Carlo simulations with random distribution of Fe and Ni atoms and magnetic interactions (up to the fourth coordination shell) from the corresponding EMTO-CPA calculations. The results for the 64-atom supercell are in parentheses.

FM	DLM-LSF		DLM-LSF-MD	
LSDA	LSDA	GGA	LSDA	GGA
620 (610)	630 (630)	710	540	630

The magnetic exchange interactions in the Heisenberg Hamiltonian are roughly proportional to the square of the magnetic moment, which explains why the choice of the exchange-correlation potential has a significant effect on the Curie temperature. However, 80–90-K difference is about 10% of the experimental Curie temperature, which is quite large. Since there is no clear consensus on which functional is best for describing the magnetism in this system, 90 K is probably the lower bound of the error bar for the DFT calculations of the Curie temperature in this system.

Another important point is that all these results are lower than the experimental Curie temperature, which ranges from 775 to 840 K. Especially the DLM-LSF results, which should account better for the magnetism near the transition point, are too low. This raises the question: is this due to the use of the CPA average magnetic interactions in the Monte Carlo modeling?

To address this question, the magnetic exchange interactions in different magnetic states and using different exchange-correlation potentials were calculated for 32- and 64-atom supercells (the results for the nearest neighbor Fe-Fe interactions in the 64-atom supercell are shown in Fig. 2) modeling random $Fe_{0.5}Ni_{0.5}$ alloy. To include the effect of thermal atomic displacements, VASP *ab initio* MD simulations were performed for a 32-atom supercell (in the FM state) at 800 K and one of the MD snapshots was also used in the magnetic exchange interaction (EMTO) and Curie temperature (Monte Carlo) calculations. In the Monte Carlo simulation, only interactions at the first four coordination shells were considered (as shown by the Monte Carlo simulations with CPA magnetic exchange interactions, the interactions beyond the fourth coordination shell have a relatively small contribution).

Table III summarizes the results for different supercell sizes and configurations. The supercell size does not have a significant effect on the Curie temperature. The supercell results for the ideal underlying fcc lattice are very close to the CPA results shown in Table II. However, the thermal atomic displacements can considerably lower the Curie temperature, as seen from the last two columns in the table where the results are based on the magnetic exchange interactions obtained from a MD snapshot. This large reduction of the Curie temperature due to the coupling of magnetic exchange interactions and thermal lattice vibrations was also observed in bcc Fe [43]. Therefore, the present *ab initio* based modeling

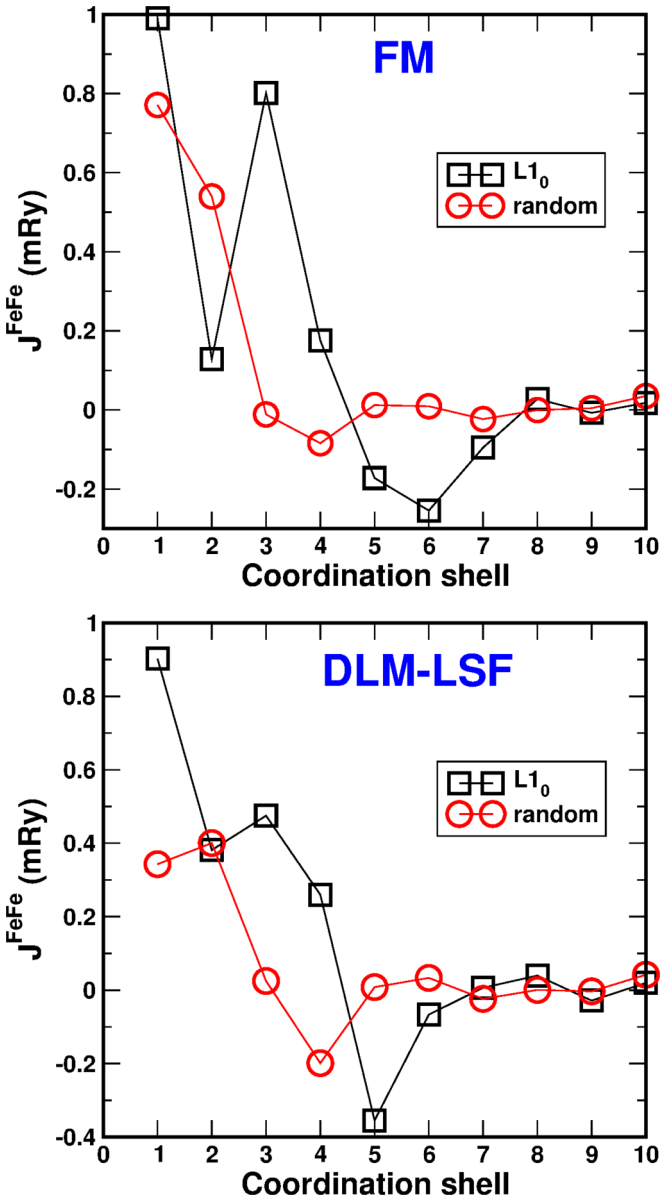

FIG. 5. The Fe-Fe magnetic exchange interactions in the ordered $L1_0$-FeNi and random $Fe_{0.5}Ni_{0.5}$ alloys in FM (top) and DLM-LSF (bottom) states (LSDA results).

predicts a Curie temperature of random $Fe_{0.5}Ni_{0.5}$ alloy that is about 200 K below its experimental value, which is a 25% error.

Another factor that may be important is the alloy configuration. The alloys in the experiment are likely not completely random, but have some degree of atomic SRO. The simplest way to analyze its effect is to calculate the magnetic exchange interactions in the $L1_0$-FeNi with different degrees of long-range order using the $L1_0$ primitive unit cell in the EMTO-CPA calculations. In the fully ordered alloy, there are no local environment effects. They become more pronounced as the long-range order parameter decreases, but as shown before, the mean-field average interactions give almost the same results as the interactions that account for the local environment dependence.

TABLE IV. Curie temperature as a function of the long-range parameter, η, in FeNi-$L1_0$ alloy. The atomic SRO at the first coordination shell, α_1, is also shown.

		DLM-LSF		FM	
η	α_1	LSDA	GGA	LSDA	GGA
1.0	−0.333	920	990	810	890
0.8	−0.267	810	890		
0.6	−0.2	740	820		
0.4	−0.133	640	730		

Figure 5 shows the effect of atomic ordering on the Fe-Fe interactions in both FM and DLM-LSF states (the Ni-Ni and Fe-Ni magnetic exchange interactions are much less affected by the ordering and are not shown). The Fe-Fe magnetic exchange interactions at the first and third coordination shells are much stronger in the ordered alloy than in the random one, while the interaction at the second coordination shell is weaker. However, the third coordination shell has a larger impact, since its coordination number is 24, compared to the second coordination shell with a coordination number of 6.

Table IV shows the Curie temperatures obtained by Monte Carlo simulations using the magnetic exchange interactions for different values of the long-range order parameter. The results indicate that atomic order leads to a significant increase of the Curie temperature. This strong dependence of the Curie temperature on the state of atomic order implies that a quantitative comparison between experiment and theory can only be done if the state of order or atomic SRO in the experiment is known.

Another important conclusion is that atomic ordering in FeNi strongly enhances ferromagnetism. This is a very general feature in fcc Fe-Ni alloys that is independent of the uncertainties of the exchange-correlation potential and the approximations in the magnetic exchange interaction calculations: when Fe atoms have Fe nearest neighbors, the local Fe-Fe interactions become antiferromagnetic, weakening ferromagnetism. Atomic ordering reduces the number of Fe nearest neighbors, thereby increasing the local magnetic moment and strengthening the ferromagnetic Fe-Fe interactions. This implies that there is a reverse effect: ferromagnetism should promote ordering. Both ordering and ferromagnetism increase the stability of the system. This will be clearly demonstrated below.

B. Effective interactions and ordering in FeNi

1. Effective chemical interaction and ordering energy

Since magnetic and chemical degrees of freedom are tightly coupled as they stem from the same electronic structure, one can expect that effective chemical interactions depend strongly on the magnetic state as well as on the local environment of sites involved in the interaction (examples of such strong dependence on the local environment in FeCr and FeCu are discussed in Refs. [44,45]). The chemical Hamiltonian (1), which will be used for the order-disorder simulations, does not account for these effects

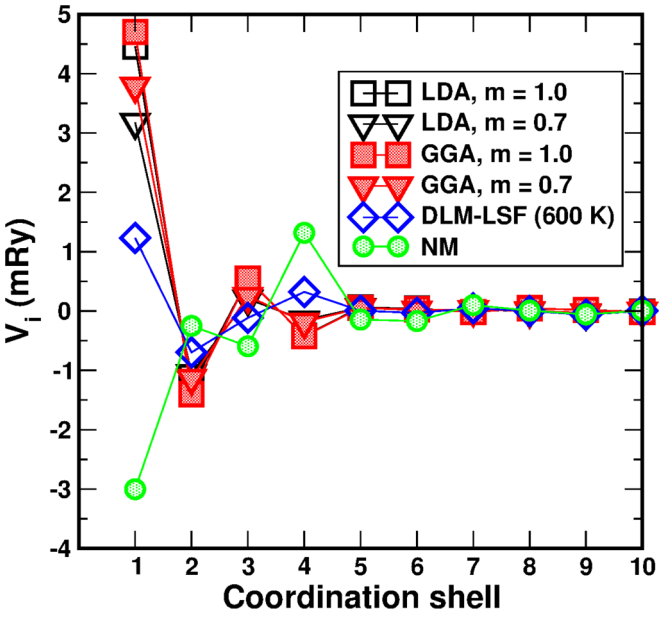

FIG. 6. SGPM effective interactions in random $Fe_{0.5}Ni_{0.5}$ alloy in the FM state with two different magnetizations (1.0 and 0.7), in the DLM-LSF (600 K) state and nonmagnetic state (without spin polarization).

and therefore the interactions in the Hamiltonian will be treated as the mean-field average.

The effective chemical interactions are calculated here by two methods: SGPM and direct supercell total energy calculations based on the Hamiltonian (1). The SGPM is a powerful tool, closely related to the magnetic force theorem, that allows one to determine interactions for any specific cluster in random alloys. The SGPM effective interactions depend on concentration, volume, and magnetic state. This makes the SGPM very efficient and convenient for studying configurational thermodynamics in magnetic systems, especially in the not fully ordered magnetic state, which is the case of FeNi at the order-disorder phase transition point.

Figure 6 shows the first ten SGPM effective pair interactions in random $Fe_{0.5}Ni_{0.5}$ alloy for different magnetic states (the interactions beyond the tenth coordination shell are small). The interactions at the first four coordination shells are the strongest (as in the case of the magnetic exchange interactions). As one can see, the magnetic state has a strong effect on the effective interactions, especially at the first and fourth coordination shells: the ordering (related to the positive interaction at the first coordination shell and negative at the second in the case of $L1_0$ structure) becomes weaker when magnetization is reduced and the system will form clusters in the nonmagnetic (NM) state.

To verify the accuracy of the SGPM and to include the strain-induced contribution to the effective interactions, a direct total energy method was applied, which is similar to the SGPM [46]. The idea is to use a supercell of a random alloy where all the atomic distribution correlation functions (corresponding to the strongest effective interactions in the system, which can be identified, for example, by the SGPM calculations) are the same as in a completely random alloy, except for one specific cluster of interest. The total energy of such a supercell can be obtained with the precision of the current DFT functionals and thus it can provide reliable results for this particular effective interaction.

TABLE V. Effective pair interactions (in nm Ry) in the NM state.

	Coordination shell			
	1	2	3	4
	256-atom supercell			
1	−3.146	0.265	−0.431	1.386
2	−3.050	−0.265		
3		−0.391		
Avg.	−3.098	−0.130	−0.431	1.386
	576-atom supercell			
	−3.078	0.010	−0.392	1.424
SGPM	−3.002	−0.025	−0.593	1.318

The effective pair interactions in the direct total energy method are determined as

$$V_p^{(2)} = \frac{2}{c(1-c)\Delta\alpha_p z_p}\Delta E_0, \tag{7}$$

where ΔE_0 is the difference of the two total energies (per atom) of supercells where all the atomic distribution functions except the atomic SRO at the p coordination shell, α_p, are the same as in a totally random alloy. The effective interactions obtained from the ideal primitive (fcc) lattice are the same as the "chemical" contribution given by the SGPM, and the effective interactions obtained from the relaxed lattice include the strain-induced contribution as well. Here, such a method has been used to calculate the effective pair interactions at the first four coordination shells.

The supercell calculations were performed for 256-[4×4×4(×4)] and 574-atom [6×6×4(×4)] supercells in the FM and NM states for the first four strongest pair interactions. Each interaction was obtained from the total energies of two supercells with positive and negative values of the atomic SRO, α_i, for the same coordination shell. In some cases, two different pairs of α_i were used to obtain a more reliable average value. Table V shows the supercell results and the SGPM effective interactions for the NM state.

The strong fluctuations of the results in the 256-atom supercell calculations for the second coordination shell are unlikely to be caused by a contribution from long-range pair or higher order cluster interactions. In all these cases, the atomic SRO parameters were very small (less than 0.005 in absolute value) for coordination shells beyond the fifth and up to the ninth. The correlation functions for the strongest three-site and four-site effective interactions were close to the random values. The exact source of these fluctuations is thus unclear.

The SGPM effective interactions and the supercell interactions agree well, considering the methodological differences and the fact that a simple expansion of the configurational energy (1) does not account for the local environment effects. The important quantity that these interactions are supposed to reproduce is the ordering energy. The $L1_0$ ordering energy from the SGPM effective interactions (pair and four-site) is 3.53 m Ry, which is in very good agreement with the VASP

TABLE VI. Effective pair interactions (in m Ry) in the FM state. The SGPM interactions here are obtained in the GGA-PBE self-consistent calculations. The SGPM* results are obtained with fixed local magnetic moments of Fe and Ni from the GGA-PBE calculations of the $L1_0$ FeNi.

	Coordination shell			
	1	2	3	4
	256-atom supercell			
1	3.659	−1.900	0.641	−0.063
2	3.653	−0.915	0.507	−0.138
3		−1.029		
4		−1.877		
Avg.	3.656	−1.430	0.574	−0.100
	576-atom supercell			
1	3.207	−1.988	0.108	−0.307
2	3.567	−2.297	−0.023	−0.496
Avg.	3.387	−2.143	0.043	−0.401
SGPM	4.702	−1.399	0.545	−0.424
SGPM*	5.526	−1.519	0.605	−0.334

TABLE VII. $L1_0$ ordering energy (in m Ry/atom) in the FM, paramagnetic (PM), and NM states. ΔE_0 are the results from direct calculations of the total energies of the $L1_0$ ordered and random alloys (on the underlying ideal fcc lattice, with the same lattice parameter, 3.591 Å). The FM and NM results for ΔE_0 are from VASP supercell calculations, while PM results are from EMTO-CPA calculations for the DLM-LSF state at 600 K. The results from the SGPM effective interactions obtained using the first 25 pair interactions and 36 strongest four-site interactions. The SGPM results in parentheses are from the first four effective pair interactions, as is the case of the results from effective interactions obtained in the VASP 256-atom (V-256) and 576-atom (V-576) supercell calculations. These interactions are presented in Tables V and VI. The SGPM* ordering energy is obtained from interactions calculated fixing the magnetic moments of Fe and Ni to those in the ordered $L1_0$-FeNi (see Table I).

	ΔE_0	SGPM	SGPM*	V-256	V-576
FM	−5.63$	−4.78$ (−4.58)	−4.93$ (−5.06)	−3.61$	−3.94$
PM	−0.38$	−0.60$ (−0.54)			
NM	3.59	3.56 (3.88)		3.96	4.07

direct supercell total energy calculations: 3.59 m Ry (supercell random alloy on the ideal fcc lattice, i.e., without local lattice relaxations).

The results for the FM state are given in Table VI. In the FM case, the agreement between SGPM and supercell results is noticeably worse than in the NM case, and the agreement between 256- and 576-atom calculations is poor for all the coordination shells except the first one. This may be because the 576-atom supercell represents a wider range of local atomic configurations than the 256-atom one. For example, in the latter case, almost all the local magnetic moments of Fe atoms are ferromagnetically aligned, while some Fe atoms (up to six in the present investigation) have had antiferromagnetic alignment of the magnetic moment with respect to the global magnetization in the 576-atom supercells. In other words, it seems that local magnetic state fluctuations leading to "antiferromagnetic" Fe atoms in the 576-atom supercells can have a noticeable effect on the effective interactions. In the case of 256-atom supercells, the fluctuations of the local composition are not that strong, which could be the reason why the SGPM effective interactions agree better with those from the 256-atom supercell calculations.

Table VII shows the $L1_0$ ordering energy in the FM state obtained in the direct calculations as well as from the SGPM and the supercell effective interactions (without local relaxations in random alloy). The contribution from the more distant coordination shells obtained from the SGPM interactions is only 0.1 m Ry/atom and the contribution from 500 effective four-site interactions is about −0.3 m Ry/atom. Both of them are relatively small. However, it is very difficult to identify the few four-site interactions that have the most impact on the ordering energy: there are many small interactions that produce a strong collective effect.

The directly calculated ordering energy in the FM state is noticeably lower than the one from the effective interactions, unlike the nonmagnetic case. This can be expected, since the magnetic state is much stronger in the $L1_0$ ordered alloy than in the random alloy. However, the effective interactions are obtained for a random alloy configuration where the ferromagnetic state is weaker than in the ordered alloy (as discussed above). Therefore, the effective interactions do not account for the stronger ferromagnetism in the ordered state, which leads to an underestimation of the ordering energy.

To see the effect of the magnetic state, one can compare the ordering energy from SGPM and SGPM* interactions. The latter are obtained by fixing the magnetic moments of Fe and Ni to those in the $L1_0$ ordered structures. Table VII shows that ferromagnetism strongly promotes atomic ordering, in contrast to what was found in Ref. [12].

2. Strain-induced interactions in the FM state

The size difference of Fe and Ni atoms is relatively small, so the energy of local lattice relaxations in random $Fe_{0.5}Ni_{0.5}$ alloy is also small: −0.41 and −0.53 m Ry/atom, obtained from 256- and 576-atom supercell calculations, respectively, in the FM state and for the fixed lattice constant. This energy can be included in the configurational thermodynamics through the strain-induced interactions. These interactions are long range and may also have contributions from multisite clusters.

Here, only the first four pairs of strain-induced interactions are calculated from the energies of the local relaxations of the supercells using Eq. (7) of the 256-atom supercells used in the calculations of the chemical interactions. The results are listed in Table VIII. They are relatively small, with the strongest one at the second coordination shell. However, the results fluctuate considerably for different sets of calculations. Unfortunately, the corresponding total energy calculations with structural optimization are very time consuming, and thus it is difficult to obtain accurate results.

TABLE VIII. Strain-induced interactions (in m Ry) in the FM state from 256-atom supercell calculations.

	Coordination shell			
	1	2	3	4
	256-atom supercell			
1	−0.422	−0.977	0.074	0.154
2	−0.514	−1.270	0.072	0.192
3		−0.119		
4		−0.239		
Avg.	−0.468	−0.651	0.073	0.173

The strain-induced interactions can be used to calculate the energy of local lattice relaxations in a random alloy as

$$E_0^{\rm rel} = \frac{1}{2}c(1-c)\sum_i z_i V_i^{\rm SI}, \tag{8}$$

where $V_i^{\rm SI}$ are the strain-induced interactions from the the ith coordination shell. The result of −0.71 m Ry/atom is a bit lower than the energy obtained in the direct calculations, but still reasonable for a qualitative estimate of their effect. Most probably, the effect of the strain-induced interactions on the order-transition temperature is going to be overestimated by additional lowering of the order-disorder transition temperature. Although the strain-induced interactions have been obtained in the fully ordered ordered FM state, the effect of reduced magnetization is expected to be small since these interactions are mostly related to the size difference of alloy components.

3. Vibrational free energy contribution to the ordering energy of FeNi at 600 K

The vibrational contribution to the free energy of random and ordered FeNi alloys in the FM state was obtained by PHONOPY code [47] using the small displacement method. The lattice constant was fixed to 3.591 Å, which corresponds to the order-disorder transition temperature at 600 K. The initial 16-atom supercell modeling random alloy (2×2×4 of the primitive fcc unit cell) was enlarged by a factor of 8 (2×2×2) in the dynamical matrix calculations. The local positions of atoms were relaxed. The initial cubic four-atom unit cell of the $L1_0$ structure was also enlarged by a factor of 8 (2×2×2) for the force constant calculations. The c/a ratio of the $L1_0$ structure was relaxed to the equilibrium value.

Similar calculations were done for the ordered $L1_2$ Ni_3Fe and random $Ni_{0.75}Fe_{0.25}$ alloys. In the latter case, the 32-atom supercell representing a random alloy [2×2×2 of the fcc cubic unit cell (×4)] was enlarged by a factor of 8 (2×2×2) in the dynamical matrix calculations. The lattice constant in both calculations was 3.556 Å, which is the experimental room temperature value. The calculations were done in the FM state.

Table IX shows the calculated vibrational free energies of FeNi and Ni_3Fe. The 300-K results for entropies in Ni_3Fe are in reasonable agreement with experimental data [48]. As reported by Li *et al.* [12] there is a substantial increase of the difference between the vibrational entropies of random and ordered alloys when going from Ni_3Fe to FeNi alloys, which is likely associated with increased concentration of Fe and related local environment effects in random alloys since this increase is mainly due to the change of the vibrational entropy of the random $Fe_{0.5}Ni_{0.5}$ alloy.

TABLE IX. Vibrational entropies and free energies (in m Ry/atom) of Ni_3Fe and FeNi alloys.

T (K)		Ordered	Random	Difference
		Ni_3Fe		
300	S	3.437	3.483	0.046
	−TS	−6.530	−6.617	−0.087
	F	−0.405	−0.496	−0.091
600	S	5.434	5.481	0.047
	F	−9.034	−9.213	−0.179
FeNi				
600	S	5.429	5.588	0.159
	F	−9.010	−9.628	−0.618

The entropy differences shown in Table IX are about half of those obtained by Li *et al.* [12] (see Supplementary Materials). This may be due to the different choices of the lattice constants in the phonon calculations. Here, the same lattice constants for the ordered and random alloys are chosen to find the contribution to the ordering energy at the experimental lattice constant where the order-disorder phase transition occurs. Although this transition is of the first order, the ordered phase should have a very similar lattice constant to the random phase during the initial stages of precipitation at the corresponding transition temperature.

At 600 K, the free energy difference between random and ordered alloys is −0.62 m Ry/atom. It is comparable to the contribution from the strain-induced interactions (or local lattice relaxations). However, it is much smaller than the ordering energy. This means that the vibrational contribution cannot change the order-disorder transition temperature by a factor of 2 as found in [11,12]. Although these results are obtained in the FM state with magnetization 1, one cannot expect a large effect when the magnetization is reduced to 0.7, which is the value at the order-disorder phase transition point.

The vibrational contribution is added to the nearest neighbor effective interactions since the main renormalization of the force constants most probably occurs at the first coordination shell [similar to Eq. (7)]:

$$V_1^{\rm vib} = \frac{2}{c(1-c)z_1\alpha_1^{\rm L1_0}}\Delta F^{\rm vib} = 2\Delta F^{\rm vib}. \tag{9}$$

Here $\alpha_1^{\rm L1_0} = -1/3$ is atomic SRO at the first coordination shell in the $L1_0$ ordered alloy and $\Delta F^{\rm vib}$ is the difference of the vibrational free energies of random and ordered FeNi at 600 K. This results in a contribution of −1.236 m Ry. Note that a similar contribution to the effective interaction for the Ni_3Fe alloy at 800 K (close to the order-disorder phase transition in this case) would be about only −0.24 m Ry, which is quite small (in the range of the error for the effective interactions), and thus it cannot affect much the theoretical results for the order-disorder transition temperature.

TABLE X. First four effective pair interactions included in MC simulations (in m Ry) for magnetization $m = 0.7$.

	Coordination shell			
	(110)	(200)	(211)	(220)
	LDA			
SGPM	3.18	−1.05	0.21	−0.15
+ vibr	1.94	−1.05	0.21	−0.15
+ vibr + si	1.48	−1.70	0.28	0.02
	GGA-PBE			
SGPM	3.79	−1.13	0.25	−0.18
+ vibr	2.55	−1.13	0.25	−0.18
+ vibr + si	2.08	−1.78	0.32	−0.01

4. The order-disorder phase transition

The order-disorder transition in FeNi is a complex phenomenon that involves the interplay of magnetic, chemical, and structural factors. To model it accurately, one needs to account for the local lattice relaxations and thermal lattice vibrations. This is impossible in the direct *ab initio* total (free) energy calculations since such a modeling also requires the proper statistical sampling of the atomic configurational degrees of freedom or, in other words, taking into consideration the atomic SRO. Neglecting the atomic SRO, as done in the CPA total energy calculations, can only provide a qualitative description of the transition.

Despite the long-standing knowledge that the single-site mean-field approximation, which is inherent to the CPA method, greatly overestimates the transition temperatures, a recent *ab initio* study of the order-disorder phase transition in FeNi using the CPA approach showed an excellent agreement with the experimental data [11]. This success needs to be explained, since the ordering energy, which is the only quantity that can be obtained from such calculations, has a rather approximate relation to the order-disorder transition temperature. A simple example below illustrates this point in the Appendix.

In this paper, the Ising-type Monte Carlo simulations are done to determine the order-disorder transition temperature using a cubic $12\times12\times12(\times4)$. Test Monte Carlo calculations with a $24\times24\times24(\times4)$ box produced essentially the same results. The temperature step in Monte Carlo simulations was 5 K. All Monte Carlo simulations were done with the effective pair interactions up to the 25th coordination shell (although all the effective interactions beyond the tenth coordination shell are less than 0.01 m Ry). In Table X, the first four strongest effective pair interactions are shown for reduced magnetization 0.7 with different contributions and obtained different exchange-correlation potentials.

The three-site interactions do not contribute to the ordering energy and practically do not affect the order-disorder transition temperature in equiatomic alloys. Thus, only the strongest four-site interactions have been included in Monte Carlo simulations in some cases. They are listed in Table XI [49]. Although the included four-site interactions change the order-disorder transition temperature, the exact effect of all the four-site interactions may be different. As has been mentioned above, a large number of relatively weak interactions produce a collectively significant effect as, for instance, is discussed in Refs. [32,50]). Including them in Monte Carlo simulations makes the calculations very time consuming and impractical. However, they cannot change the results qualitatively.

TABLE XI. The strongest four-site effective interactions (in m Ry) for magnetization $m = 0.7$. See Ref. [49] for the tetrahedra identification.

	Tetrahedron type					
	$t1$	$t2$	$t3$	$t4$	$t5$	$t6$
LDA	0.41	0.38	−0.07	−0.14	0.16	−0.15
GGA-PBE	0.29	0.29	−0.14	−0.16	0.16	−0.12

Table XII shows the order-disorder transition temperature for different sets of interactions. The choice of the exchange-correlation functional can affect the transition temperature by about 100 K, with the GGA-PBE potential increasing the transition temperature compared to the LDA potential. This effect is due to the different magnetic properties (moments and interactions) that result from the LSDA and GGA-PBE calculations (for the same lattice constant).

Table XII also reveals the strong influence of the magnetic state on the transition temperature (without the vibrational and strain-induced contributions): the transition temperature is about 1000 K in the fully ordered FM state, 600–700 K for $m = 0.7$, 500–600 K for $m = 0.6$, and below 200 K in the paramagnetic DLM-LSF state (at 600 K). This dramatic decrease of the transition temperature from the ferromagnetic to the paramagnetic state is consistent with the ordering energy in Table VII, so the opposite effect reported by Li *et al.* [12] is hard to understand.

IV. CONCLUSIONS

Accurate *ab initio* modeling of phase transitions at finite temperature in such complex itinerant magnets like FeNi is extremely challenging and can hardly be done quantitatively, at least for the phase transition temperatures: even the choice of the exchange-correlation potential significantly affects the results, and it is not clear which one is more accurate and reliable.

The problem is related to the magnetism. At 0 K and the same lattice constant, the magnetic moment of Fe is different in the LSDA and GGA-PBE (in fact, a different choice of the GGA usually leads to different results for the magnetic moment). In turn, it leads to different "magnetic" energies, which are obviously coupled with chemical ones. So, in the end, all types of interactions, magnetic and chemical, are dependent on the choice of the exchange-correlation potential. An additional problem arises at finite temperature, where an *ad hoc* modeling of magnetism is required in DFT calculations, and its accuracy is unknown.

The magnetic phase transition was found to depend on (1) the choice of the exchange-correlation functional, (2) the thermal atomic displacements, and (3) the atomic ordering.

TABLE XII. Order-disorder transition temperature obtained from SGPM interactions with different magnetization m and using different exchange-correlation potentials. All the results are obtained with the first 25 effective pair interactions. The results in parentheses are obtained including also the six strongest effective four-site SGPM interactions. For $m = 0.7$ the results with the additional vibrational contribution (+vibr) and with both vibrational and strain-induced interactions (+vibr,si) are shown.

	V					
	$m = 1.0$	$m = 0.7$			$m = 0.6$	$m = 0.0$ (DLM-LSF)
	SGPM-2	SGPM	+vibr	+vibr,si	SGPM-2	SGPM-2
LDA	970	635 (695)	530	550 (610)	530	145
GGA	1025	730 (795)	630	650 (710)	640	190

The GGA-PBE functional gave larger magnetic moments and stronger magnetic exchange interactions than the LSDA functional, resulting in a higher Curie temperature (by about 80 K). The thermal atomic displacements (at 800 K) reduced the magnetic exchange interactions and lowered the Curie temperature by about 200 K. The long-range order increased the magnetic moments, magnetic exchange interactions, and Curie temperature. However, the calculated Curie temperature in the random alloy was much lower than the experimental value, and the reason for this discrepancy was not clear. Hopefully, an *ab initio* modeling with a better description of the finite-temperature magnetic state, such as DMFT, will resolve this issue in the future.

Although the results for order-disorder phase transition seem to be in reasonable agreement with the experiment, its modeling can be considered only qualitative. Even the choice of the exchange-correlation potential changes the result by 100 K. However, one result can hardly be different in a more thorough and accurate modeling: the atomic ordering is much stronger in the ferromagnetic state than in the paramagnetic one, which is also the result of the direct *ab initio* calculations of the ordering energy presented in Table VII. This is a common feature of Fe-Ni alloys, which can be explained by the strong influence of the nearest neighbor Ni atoms on the magnetic state of the Fe atoms: the more Ni atoms surround an Fe atom, the more it prefers the ferromagnetic state, which also enhances the ordering tendency.

ACKNOWLEDGMENTS

The DFT simulations were performed on resources provided by the National Academic Infrastructure for Supercomputing in Sweden at PDC (Stockholm) and NSC (Linköping). The author also gratefully acknowledges financial support under the scope of the COMET program within the K2 Center "Integrated Computational Material, Process and Product Engineering" (Project No. 859480). This program is supported by the Austrian Federal Ministries for 718 Climate Action, Environment, Energy, Mobility, Innovation, and Technology (BMK) and for Digital and Economic Affairs (BMDW), represented by the Austrian research funding association (FFG), and the federal states of Styria, Upper Austria, and Tyrol.

APPENDIX: SRO EFFECT IN THE $L1_0$ ORDER-DISORDER PHASE TRANSITION

Consider two systems with the same $L1_0$ ordering energy of -1000 K. The first system has only one effective interaction at the first coordination shell, while the second system has two effective interactions at the first and second coordination shells. The ordering energy can be expressed as

$$E_{\text{ord}} = \frac{1}{2}c(1-c)\sum_i \alpha_i^{L1_0} z_i V_i, \tag{A1}$$

where $\alpha_i^{L1_0} = -\frac{1}{3}$ and 1 are the atomic SRO at the first and second coordination shells. This equation was previously used in Eqs. (7) and (9). From this equation, one finds that $V_1 = 2000$ K for the first system. For the second system, one can assume that $|V_1/V_2| = 4$ and $V_2 < 0$, which is similar

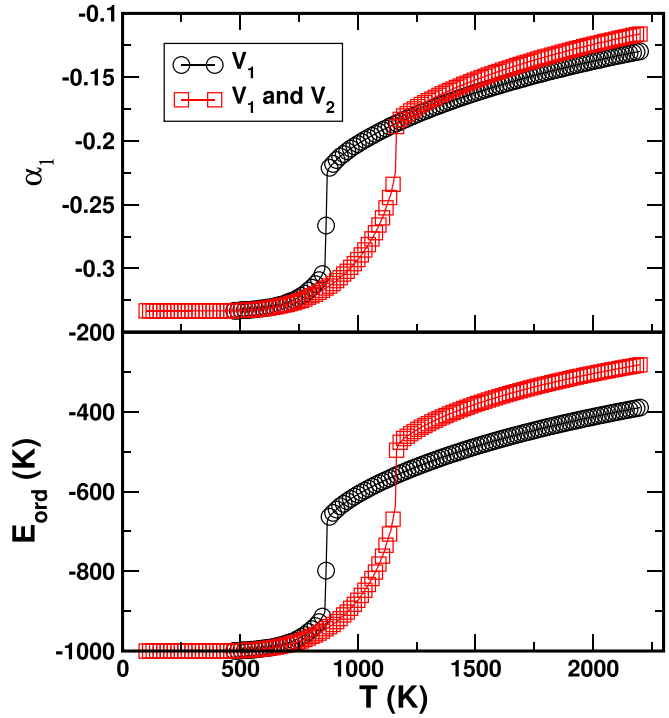

FIG. 7. Atomic SRO at the first coordination shell (top) and the corresponding ordering energy (bottom) obtained in Monte Carlo simulations with one and two effective interactions which provide the same $L1_0$ ordering energy (-1000 K).

to the SGPM interactions in FeNi alloys. Then the effective interactions are $V_1 = 1454.5$ and $V_2 = -363.6$ K.

The single-site mean-field approximation yields the same order-disorder transition temperature of about 1320 K for both systems with the same ordering energy of −1000 K. However, the Monte Carlo simulations reveal a significant difference: the first system has a transition temperature of 850 K, while the second system has a transition temperature of 1155 K. This means that the ordering energy alone does not determine the order-disorder transition temperature. There may exist other sets of interactions that have a lower ordering energy than a given set, but a higher transition temperature. At the same time, the effective interactions used in the Ising model have a clear physical meaning and values for specific alloys and they can be directly obtained from *ab initio* simulations, for instance, using the SGPM.

Figure 7 shows the atomic SRO parameter at the first coordination shell (top panel) and the ordering energy (bottom panel) for the two cases discussed above. It illustrates the importance of the atomic SRO in calculating the transition temperature. The atomic SRO parameter is large in both cases even at temperatures much higher than the transition point, which is marked by a sharp change in the atomic SRO and the ordering energy.

The energy associated with the atomic SRO (above the transition point) is also significant: it accounts for almost half of the total $L1_0$ ordering energy at temperatures twice as high as the transition point. This energy is ignored in the single-site mean-field simulations and the CPA *ab initio* calculations. Therefore, if the transition temperature obtained from these methods agrees well with the experiment, there must be another large error that compensates for the error from neglecting the atomic SRO effects. Figure 7 also explains why the transition temperature is higher in the second model: the atomic SRO energy in the random state is noticeably higher in the second case than in the first one.

[1] P. Wasilewski, Phys. Earth Planet. Inter. **52**, 150 (1988).
[2] L. H. Lewis *et al.*, J. Phys.: Condens. Matter **26**, 064213 (2014).
[3] Y. P. Ivanov, B. Sarac, S. V. Ketov, J. Eckert, and A. L. Greer, Adv. Sci. **10**, 2204315 (2023).
[4] J. Paulevé, D. Dautreppe, J. Laugier, and L. Néel, J. Phys. Radium **23**, 841 (1962).
[5] J. Crangle and G. C. Hallam, Proc. R. Soc. A **272**, 119 (1963).
[6] Y. Tanji, H. Asano, and H. Moriya, Tohoku Univ. Ser. A: Phys. Chem. Metall. **24**, 205 (1972).
[7] L. H. Lewis, F. E. Pinkerton, N. Bordeaux, A. Mubarok, E. Poirier, J. I. Goldstein, *et al.*, IEEE Magn. Lett. **5**, 1 (2014).
[8] T. Nagata, J. A. Danon, and M. Funaki, Mem. Natl Inst. Polar Res., Spec. Issue **46**, 263 (1987).
[9] T. Mohri, Y. Chen, and Y. Jufuku, Calphad **33**, 244 (2009).
[10] A. Edström, J. Chico, A. Jakobsson, A. Bergman, and J. Rusz, Phys. Rev. B **90**, 014402 (2014).
[11] L.-Y. Tian, H. Levämäki, O. Eriksson, K. Kokko, À. Nagy, E. K. Délczeg-Czirják, and L. Vitos, Sci. Rep. **9**, 8172 (2019).
[12] K. Li, C.-C. Fu, M. Nastar, F. Soisson, and M. Y. Lavrentiev, Phys. Rev. B **106**, 024106 (2022).
[13] A. V. Ruban, S. Khmelevskyi, P. Mohn, and B. Johansson, Phys. Rev. B **76**, 014420 (2007).
[14] M. Ekholm, H. Zapolsky, A. V. Ruban, I. Vernyhora, D. Ledue, and I. A. Abrikosov, Phys. Rev. Lett. **105**, 167208 (2010).
[15] D. Benea, J. Minar, H. Ebert, and L. Chioncel, Phys. Rev. B **97**, 144408 (2018).
[16] A. S. Belozerov, A. A. Katanin, and V. I. Anisimov, J. Phys.: Condens. Matter **32**, 385601 (2020).
[17] P. E. Blöchl, Phys. Rev. B **50**, 17953 (1994).
[18] G. Kresse and D. Joubert, Phys. Rev. B **59**, 1758 (1999).
[19] G. Kresse and J. Hafner, Phys. Rev. B **48**, 13115 (1993).
[20] G. Kresse and J. Furthmüller, Comput. Mater. Sci. **6**, 15 (1996).
[21] J. P. Perdew, K. Burke, and M. Ernzerhof, Phys. Rev. Lett. **77**, 3865 (1996).
[22] P. Soven, Phys. Rev. **156**, 809 (1967); B. L. Gyorffy, Phys. Rev. B **5**, 2382 (1972).
[23] I. A. Abrikosov, A. M. N. Niklasson, S. I. Simak, B. Johansson, A. V. Ruban, and H. L. Skriver, Phys. Rev. Lett. **76**, 4203 (1996); I. A. Abrikosov, S. I. Simak, B. Johansson, A. V. Ruban, and H. L. Skriver, Phys. Rev. B **56**, 9319 (1997).
[24] O. K. Andersen, O. Jepsen, and G. Krier, in *Lectures on Methods of Electronic Structure Calculations*, edited by V. Kumar, O. K. Andersen, and A. Mookerjee (World Scientific, Singapore, 1994), p. 63.
[25] L. Vitos, *Computational Quantum Mechanics for Materials Engineers* (Springer-Verlag, New York, 2007).
[26] L. Vitos, I. A. Abrikosov, and B. Johansson, Phys. Rev. Lett. **87**, 156401 (2001).
[27] O. E. Peil, A. V. Ruban, and B. Johansson, Phys. Rev. B **85**, 165140 (2012).
[28] The Lyngby version of the EMTO code properly takes into consideration electrostatics in random alloys in contrast to other existing versions. It is distributed by A. V. Ruban.
[29] A. V. Ruban and H. L. Skriver, Phys. Rev. B **66**, 024201 (2002); A. V. Ruban, S. I. Simak, P. A. Korzhavyi, and H. L. Skriver, **66**, 024202 (2002).
[30] F. Ducastelle and F. Gautier, J. Phys. F **6**, 2039 (1976).
[31] F. Ducastelle, *Order and Phase Stability in Alloys* (North-Holland, Amsterdam, 1991).
[32] A. V. Ruban, S. Shallcross, S. I. Simak, and H. L. Skriver, Phys. Rev. B **70**, 125115 (2004).
[33] A. Liechtenstein, M. I. Katsnelson, and V. A. Gubanov, J. Phys. F **14**, L125 (1984).
[34] A. Liechtenstein, M. I. Katsnelson, V. P. Antropov, and V. A. Gubanov, J. Magn. Magn. Mater. **67**, 65 (1987).
[35] A. V. Ruban and M. Dehghani, Phys. Rev. B **94**, 104111 (2016).
[36] J. P. Perdew and Y. Wang, Phys. Rev. B **45**, 13244 (1992).
[37] M. Cyrot, Phys. Rev. Lett. **25**, 871 (1970); J. Phys. France **33**, 125 (1972).
[38] B. L. Gyorffy, A. J. Pindor, J. B. Staunton, G. M. Stocks, and H. Winter, J. Phys. F **15**, 1337 (1985).
[39] A. V. Ruban, A. B. Belonoshko, and N. V. Skorodumova, Phys. Rev. B **87**, 014405 (2013).
[40] M. Hayase, M. Shiga, and Y. Nakamura, J. Phys. Soc. Jpn. **34**, 925 (1973)

[41] A. V. Ruban, M. I. Katsnelson, W. Olovsson, S. I. Simak, and I. A. Abrikosov, Phys. Rev. B **71**, 054402 (2005)

[42] I. A. Abrikosov, A. E. Kissavos, F. Liot, B. Alling, S. I. Simak, O. Peil, and A. V. Ruban, Phys. Rev. B **76**, 014434 (2007).

[43] A. V. Ruban and O. E. Peil, Phys. Rev. B **97**, 174426 (2018).

[44] P. A. Korzhavyi, A. V. Ruban, J. Odqvist, J.-O. Nilsson, and B. Johansson, Phys. Rev. B **79**, 054202 (2009).

[45] O. I. Gorbatov, I. K. Razumov, Y. N. Gornostyrev, V. I. Razumovskiy, P. A. Korzhavyi, and A. V. Ruban, Phys. Rev. B **88**, 174113 (2013).

[46] M. Dehghani, A. V. Ruban, N. Abdoshahi, D. Holec, and J. Spitaler, Comput. Mater. Sci. **205**, 111163 (2022).

[47] A. Togo, L. Chaput, T. Tadano, and I. Tanaka, J. Phys.: Condens. Matter **35**, 353001 (2023); A. Togo, J. Phys. Soc. Jpn. **92**, 012001 (2023).

[48] M. S. Lucas, L. Mauger, J. A. Munoz, I. Halevy, J. Horwath, S. L. Semiatin, S. O. Leontsev, M. B. Stone, D. L. Abernathy, Yuming Xiao, Paul Chow, and B. Fultz, J. Appl. Phys. **113**, 17A308 (2013).

[49] Tetrahedrons are uniquely defined by a set of three vectors with a common origin. One can also use the six-index form, where each index identifies the coordination shells of a side of the tetrahedron. The sequence of indices is fixed: the first four indices are for the sides going from an initial vertex through the rest of the vertices and returning to the initial vertex. The last two indices are coordination shells of the other two sides. Here, $t1 = \{(-1,-1,0),(-1,0,1),(0,-1,1)\}$—this is the tetrahedron of the nearest neighbors or (111111) in the index form; $t2 = \{(-1,-1,0),(-1,0,1),(-1,0,-1)\}$—this is the tetrahedron, whose one side is the second coordination shell (111112); $t3 = \{(-1,-1,0),(-1,1,0),(-2,0,0)\}$—there are two sides which correspond to the second coordination shell (112211); $t4 = \{(-1,-1,0),(-1,0,1),(0,-1,-1)\}$—this is the tetrahedron with one side, which is the third coordination shell (111113); $t5 = \{(1,1,0),(1,0,-1),(-1,0,1)\}$ or (111134); $t6 = \{(1,1,0),(1,-1,0),(-1,1,0)\}$ or (111224). Here, the vectors are in the units of a half of the fcc lattice constant.

[50] A. V. Ruban and I. A. Abrikosov, Rep. Prog. Phys. **71**, 046501 (2008).